Observation of Dynamic Interaction of Vortices with Pinning Centers by Lorentz Microscopy

Tsuyoshi Matsuda, Ken Harada, Hiroto Kasai, Osamu Kamimura, Akira Tonomura*

When a magnetic field penetrates a superconductor, it forms lattices of thin filaments called magnetic vortices. If a current is applied, these vortices move if not pinned down, destroying the superconductivity. The spatiotemporal behavior of the vortices was observed in a niobium film with a square lattice of defects made by ion irradiation. The vortices formed a domain of lattices. When the intensity of the applied magnetic field was decreased, the vortices were driven out of the film across its edges; when the intensity was increased, the vortices were driven into the film. The lattice exhibited brief and intermittent flow in "rivers" along domain boundaries. The rivers did not always flow along the same paths because new lattice domain configurations emerged whenever the flow stopped.

An applied magnetic field penetrates a type II superconductor in the form of thin filaments called vortices. An electric current can flow without resistance only when the vortices are fixed by pinning centers against the Lorentz forces exerted by the current; otherwise, the motion of the vortices generates voltage, and the resultant heat is likely to destroy the superconducting state. For instance, no net pinning would arise if pinning centers were distributed randomly and were so weak as to leave the vortex lattice rigid; in this case, the forces on the whole lattice at different centers would add up to zero. Thus, the whole lattice would translate freely if it were not deformed, either elastically (without tearing) or plastically (split into domains).

What happens when strong pinning centers exist? Does the vortex lattice flow only with elastic distortions that fluctuate with time, large at some instants and small at others? Or does the lattice break down plastically into blocks, some moving and others standing still? Obtaining a clear picture of the pinning is not only important for practical applications of superconductors but also relevant to other physics problems, such as charge- and spin-density waves and Wigner crystals, in which a driven elastic medium exhibits plastic flows with tears and rips as it interacts with a rigid substrate.

Several investigations into this problem of plastic flow have been reported. Anderson (*1*) introduced the concept of the flux bundle, a collection of vortices thermally depinned from pinning centers and moving in a bundle, in flux creep; this concept was used to interpret the voltage noises observed during flux flow (*2*). Studies of such collective depinning and creep of vortices are summarized in (*3*). The vortex dynamics that should arise when a superconductor is slowly driven to the threshold of instability were recently characterized as vortex avalanches, in analogy to the avalanches observed in sandpiles (*4*, *5*). More recently, the spatial disorder in the vortex lattice that takes place when a transport current is applied was observed through small-angle neutron scattering (*5*). However, the microscopic behaviors of vortices have been inaccessible to direct spatiotemporal observations. Here, we observed the dynamics of vortices interacting with pinning centers in real time by Lorentz microscopy (*6*) as they were driven by a gradient in the vortex density that arose when a decrease in the applied magnetic field intensity drove the vortices out of a superconducting film across its edges, or when an increase in the field intensity had the opposite effect. The features of the vortex motion mentioned above were seen.

Niobium samples were prepared by chemically etching a rolled film, 15 μm thick, which was annealed at 2200°C for 10 min to increase the grain size to ~300 μm in diameter. A region of the film that was ~1000 Å thick was chosen for observation. To clearly see the effects of pinning centers on the vortex dynamics, we produced a 4 × 4 rectangular lattice (spacing, 3.3 μm) of strong centers by irradiating the chosen region with a focused 30-keV Ga ion beam (diameter, 200 Å) from a Hitachi Focused Ion Beam Machine (FB-2000). Transmission electron microscopy revealed that at each of the 4 × 4 sites, the ion beam produced a pit 400 Å in diameter and a few hundred angstroms in depth, surrounded by a region of entangled dislocations 3000 Å in diameter. The whole region acts as a pinning center and is termed a defect.

The film sample was placed in a low-temperature specimen stage in a 300-kV field-emission transmission electron microscope so that its surface formed a 45° angle with both the incident electron beam and the applied magnetic field *B*. The objective lens of the microscope was replaced by an intermediate lens to make an out-of-focus image—that is, a Lorentz micrograph—in which the vortices appear as spots of dark-bright contrasts (*7*) because the incident parallel beam of electrons is slightly deflected when passing through a vortex and is displaced on the observation plane (Fig. 1). The out-of-focus distance appropriate for the Lorentz microscopy was 10 to 30 mm, and the image magnification was ×1000 to ×2000.

Examples of such Lorentz micrographs are shown in Fig. 2. In Fig. 2A, the sample was in the normal state, and only the black image of a defect can be seen. The black or white fringes running vertically are called bend contours; they arise from the Bragg reflections around a line along which the film is slightly bent. The shift of the contours between A and B in Fig. 2 is

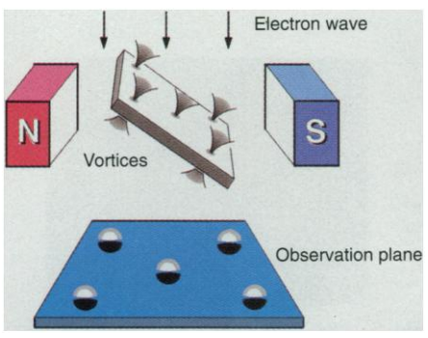

Fig. 1. Experimental arrangement for observation of vortices and defects by Lorentz microscopy. Electrons transmitted through a vortex are deflected by its magnetic field and are displaced in the observation plane. The orientation of *B* can be discerned from the orientation of the line dividing the dark-bright contrast.

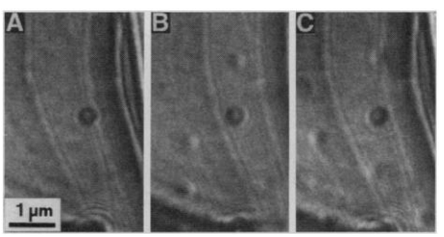

Fig. 2. Lorentz micrographs of a Nb thin film (T_c = 9.2 K) with a defect. (**A**) B = 5 G, T = 10 K; (**B**) B = 5 G, T = 4.5 K; and (**C**) B = −5 G, T = 4.5 K. Only the out-of-focus image of the defect can be seen in (A), whereas vortex images of dark-bright contrasts can also be seen in (B) and (C). Although the intensity distribution of the defect image is symmetric in (A), it is asymmetric in (B) and (C), thus showing that a vortex is trapped in the defect. The orientation of the dark-bright contrast of the image in (C) is reversed from that in (B), as expected when the direction of *B* is reversed.

Advanced Research Laboratory, Hitachi Ltd., Hatoyama, Saitama 350-03, Japan.

*To whom correspondence should be addressed.

attributable to a change in the incident angle of the electron beam to the crystal plane, which is caused by changes in experimental conditions such as B and the sample temperature T.

At T = 4.5 K and B = 5 G, three vortex images appeared, all with the bright side on the right (Fig. 2B). Because the image of the defect is also bright on its right side (though only slightly), the implication is that the defect has trapped a vortex. This interpretation was confirmed by reversing the orientation of B; in Fig. 2C, the bright sides of both the defect and vortex images are now on the left.

Using the technique of simultaneous observation of vortices and defects, we first studied how defects affected the static configuration of vortices, and then how vortices flowed through defects. With increasing B, the vortices formed lattices that became more regular; that is, the vortices repelling each other became more tightly packed (see Fig. 3). However, the vortices tended to be trapped by the defects, so that they did not form a single regular lattice but rather several domains of lattices because of the existence of the defects (Fig. 3, B and C).

The lattice became more regular as T increased. The pinning centers that existed in regions without irradiation became ineffective above T = 7 K, which implied that the pinning forces weakened at higher temperatures. Although the pinning by the defects also became weaker at T = 9 K, its effect was still recognizable. This is clearly seen in Fig. 4, where T was increased from 4.5 to 9 K with B fixed at 75 G. The random vortex configuration at 4.5 K was attributable to both kinds of pinning centers (Fig. 4A). At 7.5 K, the vortex lattice was disturbed only in the neighborhoods of the defects, which showed that the pinning centers other than those attributable to the defects became ineffective (Fig. 4B). At T = 9 K, the vortices formed a nearly perfect lattice with only slight distortions around the defects (Fig. 4C), which showed that the pinning by the defects became weak as well (the vortex images here are appreciably blurred because of the high temperature).

We next observed the dynamics of vortices in two experiments (*8*). The first experiment

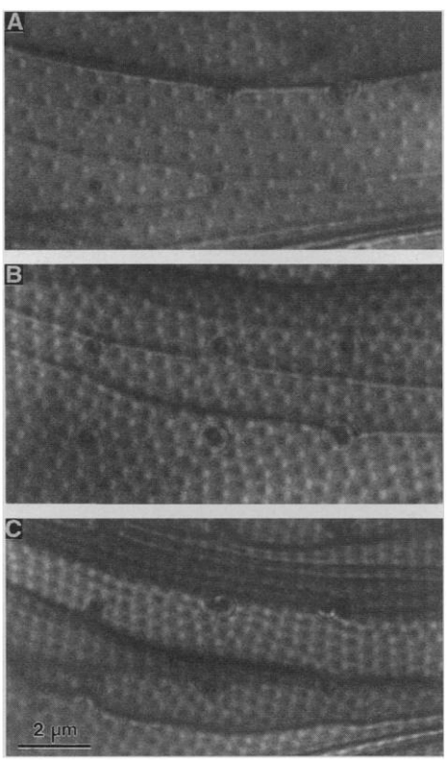

Fig. 3. Magnetic field dependence of vortex configuration near defects at T = 7 K. (**A**) B = 41 G; (**B**) B = 78 G; and (**C**) B = 106 G. When B is increased, vortices tend to form closely packed lattice domains, but the lattices have domain boundaries and dislocations near the defects.

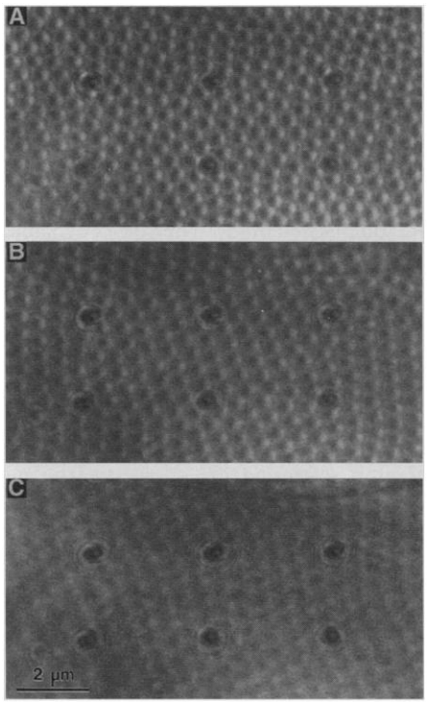

Fig. 4. Temperature dependence of vortex configuration near defects at B = 75 G. (**A**) T = 4.5 K; (**B**) T = 7.5 K; and (**C**) T = 9 K. When T is increased, the pinning effect decreases. In (A), vortices are scattered randomly. In (B), the pinning effect of the irradiation defects becomes dominant, and the vortex lattice domains have boundaries near the defects. In (C), vortices form an almost perfect lattice, but the lattice lines are still tilted at the defects.

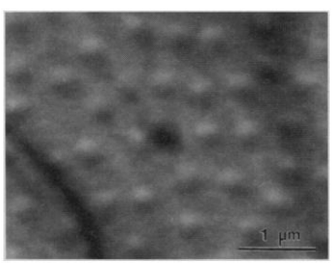

Fig. 5. Video frame of sparse vortices detouring a defect. Vortex images of dark-bright contrasts can be seen surrounding the dark image of the defect in the center of the picture. The white spot on the left side of the defect image indicates that a vortex is trapped there. The vortices hopping from the upper left to the lower right must detour this defect [see the video clip (*8*)].

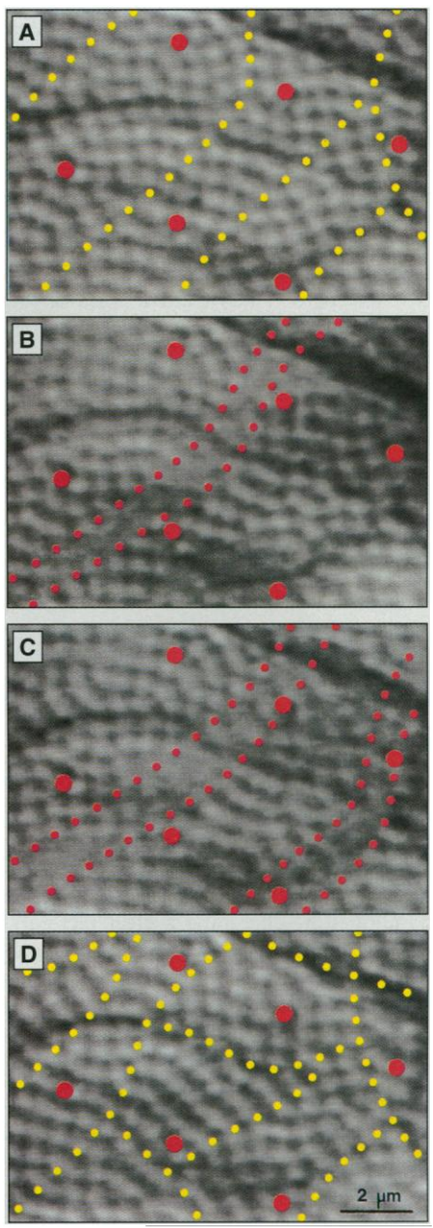

Fig. 6. Video frames of vortex lattices. (**A**) t = 0.0 s. Vortex lattices have domain boundaries near the defects (red); some of these boundaries are shown by yellow dotted lines. (**B**) t = 0.27 s. Vortices suddenly start to flow like avalanches, forming a river (between two red dotted lines) along one of the domain boundaries shown in (A). (**C**) t = 0.43 s. Another river starts flowing. (**D**) t = 0.80 s. The vortex flow stops, and a new configuration of vortex lattices is formed.

concerned the motion of sparse vortices. In the initial state, $T > T_c = 9.2$ K and $B = 0$. After cooling the sample film below T_c, we applied $B = 80$ G and observed the vortices entering the film from its edges. These sparse vortices flowed on average in the direction perpendicular to the sample edges; hence, they were driven by the gradient in the vortex density, although individual vortices often hopped in scattered directions. The effect of the gradient in film thickness was appreciable only in the case of gentle vortex flows such as flux creep. The vortex hoppings were not completely independent from each other because a vortex hopping was often triggered by an approaching vortex. In the cases where a vortex was trapped in a defect (Fig. 5), the ensuing vortices would typically make detours to avoid the defect. Only rarely did collisions occur; sometimes an oncoming vortex recoiled after collision, and sometimes an oncoming vortex was trapped for a few seconds, followed by a release of a single vortex. These observations showed that the state of two vortices trapped in one defect should be unstable, as expected. No such correlations were found in the direction orthogonal to the direction of motion.

The second experiment concerned the case in which vortices are closely packed to form lattice domains. We applied $B = 180$ G to the sample at $T > T_c$, cooled the sample to $T = 4.5$ K to find the lattice-domain formation, and then reduced B to 85 G. After the lattice domains relaxed, the sample temperature was gradually raised to let the lattice domains move freely; they then exhibited more complicated and seemingly irreproducible motion in some cases.

A typical example is shown in Fig. 6. Just before the vortex flow began, the vortices formed lattice domains at 6 K (Fig. 6A). The domain size depended on experimental conditions; it was typically a few micrometers in diameter and contained 5×5 vortices. Each domain appeared to be pinned by the defects (Fig. 6A). The vortices remained stationary for a while, then suddenly began moving in "rivers" like avalanches near some domain boundaries (Fig. 6B). When vortices flowed in rivers, they became disordered. With an exposure time of 1/30 s (Fig. 6B), those vortices that moved were blurred and could only be seen as a river. The appearance of the river changed a little after 0.16 s (Fig. 6C). When the flow stopped, a new configuration of vortex lattices emerged (Fig. 6D), and domain boundaries were formed at different locations, which in turn triggered new avalanches. The duration of the flow depended on conditions but was generally <1 s. The velocity of a vortex hopping was on the order of 1 $\mu m\ s^{-1}$.

The rivers flowed along the domain boundaries that were located near the defects; the vortex river in Fig. 6B emerged along the domain boundary located near the upper middle defect in Fig. 6A. At higher temperatures, the rivers became wider until the whole vortex lattice started to flow, keeping its form unchanged. These observations indicate that we visually monitored the transition from plastic to elastic flow.

REFERENCES AND NOTES

1. P. W. Anderson, *Phys. Rev. Lett.* **9**, 309 (1962).
2. G. J. Van Gurp, *Phys. Rev.* **166**, 436 (1968).
3. G. Blatter *et al.*, *Rev. Mod. Phys.* **66**, 1125 (1994).
4. S. Field *et al.*, *Phys. Rev. Lett.* **74**, 1206 (1995).
5. U. Yaron *et al.*, *Nature* **376**, 753 (1995).
6. K. Harada *et al.*, *ibid.* **360**, 51 (1992).
7. A. Tonomura, *Electron Holography* (Springer, Heidelberg, 1993).
8. A video clip is available at *Science*'s Beyond the Printed Page site on the World Wide Web: <http://www.aaas.org/science/beyond.htm>.

9. We thank H. Hirose for assistance in irradiating an ion beam to Nb samples and H. Ezawa, C. N. Yang, and Y. S. Ono for valuable discussions and comments.

30 August 1995; accepted 12 December 1995

Understanding the Catalytic Behavior of Zeolites: A First-Principles Study of the Adsorption of Methanol

Rajiv Shah,* M. C. Payne, M.-H. Lee, Julian D. Gale

Zeolites are microporous aluminosilicate materials used as industrial catalysts, and there is much interest in understanding their catalytic behavior. The adsorption of methanol in the catalytically active zeolite chabazite and in sodalite was examined by performing ab initio calculations within periodic boundary conditions. A direct correlation between zeolite structure and chemical activation of the adsorbate was found. Methanol was protonated without an activation energy by a Brønsted acid site, provided the molecule was situated in the eight-ring window of chabazite, whereas the same molecule was only physisorbed in more open cage regions, such as those found in sodalite.

Microporous materials are powerful industrial catalysts, combining acidity with shape selectivity for reactants, products, and their intervening transition states (*1*). Amongst the wealth of chemical reactions catalyzed by these materials, one of the most important is the conversion of methanol, initially to dimethyl ether and subsequently to gasoline (*2*). Many experimental studies have characterized intermediate species of this reaction in situ (*3*), but we can still only speculate about the true mechanism. Methanol is known from infrared spectroscopy (*4*) to be initially adsorbed at acid sites in the zeolite framework, but the interpretation of such data in terms of either physisorbed methanol or chemisorbed methoxonium species (Fig. 1) is still a matter for debate (*5*).

There has been much interest in the use of quantum mechanical methods to determine the energetics of proton transfer from the zeolite framework to methanol, because this is believed to be the first step in the activation of the adsorbate. Most of these studies have used cluster methods, in which a small fragment of the zeolite is extracted and dangling bonds are saturated with hydrogen. By using a variety of ab initio techniques, it has been shown that methanol is physisorbed and that the methoxonium ion is unstable, representing a transition state for the exchange of hydrogen between two oxygens (*6*, *7*). However, most of these calculations represent only the local bonding interaction and neglect the long-range electrostatic potential, which could have a considerable effect given the partially ionic nature of aluminosilicates. Furthermore, such cluster models are often not specific to any one zeolite structure, and therefore the results cannot explain the different catalytic activities observed with varying framework topologies.

Recent advances in massively parallel computing, coupled with improved algorithms (*8*), have greatly increased the scope of first-principles quantum mechanical calculations for periodic systems, allowing investigation of the mechanism of zeolite catalysis. We have used such techniques to address the question of methanol adsorp-

R. Shah, M. C. Payne, M.-H. Lee, Cavendish Laboratory (TCM), Madingley Road, Cambridge CB3 0HE, UK.
J. D. Gale, Department of Chemistry, Imperial College, South Kensington SW7 2AY, UK.

*To whom correspondence should be addressed.

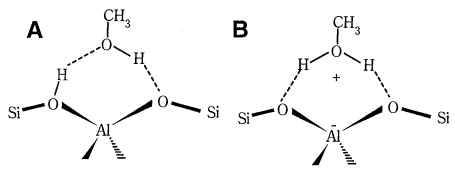

Fig. 1. Schematic illustration of the two possible adsorption complexes of methanol at an acid site (**A**) physisorbed with no proton transfer and (**B**) chemisorbed with proton transferred to form a methoxonium cation.